# Low Velocity Impact of Marine Composites: Experiments and Theory


**Valentina Lopresto, Ilaria Papa, Vito Pagliarulo, Pietro Russo, and Maurizio Porfiri**

## 1 Introduction

Several elements of naval and aerospace structures are regularly subjected to impact loading at room and low temperatures. Variations in the temperature are responsible for dramatic changes in the onset, architecture, and mechanics of damage [1–8]. Particularly relevant is to elucidate the dynamic response of lightweight composite materials, whose integration in marine vessels and aircraft is steadily growing [9–18]. In these applications, impact loading may trigger complex fluid-structure interactions.

Motivated by limited experimental evidence in the technical literature, this chapter presents a comprehensive database which can be used by high-end practitioners in naval and aerospace engineering, along with experimental and theoretical insight that can support an improved understanding of the dynamic response of composites. Such an improved understanding is critical for designing effective

V. Lopresto (✉) · I. Papa
Department of Chemical, Materials and Production Engineering, University of Naples Federico II, Naples, Italy
e-mail: lopresto@unina.it; ilaria.papa@unina.it

V. Pagliarulo
CNR National Research Council, ICIB, Institute of Cybernetics, Pozzuoli, NA, Italy
e-mail: vito.pagliarulo@cnr.it

P. Russo
CNR National Research Council, Institute for Polymers, Composites and Biomaterials, Pozzuoli, NA, Italy
e-mail: pietro.russo@unina.it

M. Porfiri
Department of Mechanical and Aerospace Engineering and Department of Biomedical Engineering, New York University Tandon School of Engineering, Brooklyn, NY, USA
e-mail: mporfiri@nyu.edu



S. W. Lee (ed.), *Advances in Thick Section Composite and Sandwich Structures*,
https://doi.org/10.1007/978-3-030-31065-3_8

manufacturing techniques to enhance the toughness of the matrix or the inter-ply interface.

Properties of composite laminates with plastic matrices at different temperatures have been extensively investigated, focusing on the onset and mechanics of damage. For example, changes of material properties in response to temperature variations were studied in [1] by Howard and Hollaway. In [2], Shindo et al. investigated the thermal mechanical response of non-metallic woven composites with temperature-dependent properties. A finite element method was used to explore the influence of crack formation, residual thermal stresses, and weave curvature on the mechanical performance of glass–epoxy laminates at low temperatures. The tensile properties of a glass/epoxy composite subjected to thermo-mechanical cyclic loads at low temperatures (up to 10 cycles) from room temperature (r. t.) to −50 °C, to −100 °C, and to −150 °C (c. t.) were studied in [3], using an environmental test chamber. Therein, Kim et al. demonstrated that the tensile stiffness significantly increases with decreasing temperature and the tensile strength decreases with decreasing temperature, while thermo-mechanical cycling plays a secondary role. In [4], Sefrani et al. presented an experimental analysis on the effect of temperature on both the stiffness and the damping of glass fiber laminates. Their experimental results indicate that mechanical properties are nearly constant up to the glass transition temperature, where the damping increased sharply in a rather small temperature interval.

Experimental tests on aramid/epoxy composite samples reinforced with glass fibers were performed in [5] using the Charpy impact method. The effects of the fiber volume fraction and the temperature on the impact toughness were tested. Impact damage was observed using a microscope at a magnification of 100. Experimental results indicate a modest increase of impact toughness of composite samples with increasing temperature in the interval − 40 °C−−10 °C. This is followed by a larger increase of the impact toughness with increasing temperature from −10 °C to room temperature. The aramid/epoxy system was observed to exhibit a higher impact toughness than glass/epoxy for all the tested temperatures [6–8]. Fiber failure was found in the composite sample. Increasing the fiber fraction volume decreases the impact toughness of glass and aramid/epoxy composites.

While many studies have characterized the properties of polymer composite materials at different temperatures, only few of them examined the influence of the temperature on the impact response. Filling this gap in knowledge is one of the key objectives of this chapter, which brings forward the investigation of the impact behavior of composite laminates of different thickness, in air and in the presence of water. Another objective of this chapter is to present a mechanics-based understanding of the fluid-structure interaction occurring during impact in the present of the water. A physically-based understanding of the fluid-structure interaction will help, in fact, to clarify the process of load redistribution during impact, inform the interpretation of empirical observations, and assist in the design of future experiments.

With respect to Navy-relevant research, it is crucial to simulate real conditions for the navigation in arctic environments, which calls for experimentally proxying complex fluid-interactions at extreme temperature. If a panel is supported by water

instead of being in air, damage will be triggered by different load distributions [9]. In the case of water-backing, further variations will occur if the loading is exerted from the water or the air side, and variations in the boundary conditions could further add to the complexity of the impact. However, only a few studies [10–13] have examined the behavior of composite laminates subject to impact at low temperature or [14–18] have tackled the problem of the fluid-structure interaction. To the best of our knowledge, the combination of low temperature and fluid-structure interaction is an untapped area of research.

Low velocity impact is one of the most subtle threats to composite materials [19–26]. Due to weak bonds between the plies, even small energies imparted by out-of-plane loads can result in hardly detectable damages, such as matrix cracks, delamination, and fiber breakage. In turn, these damages will cause considerable stiffness and strength losses in tension, and, even more, in compression, thereby severely reducing structural integrity. Hence, it is crucial to understand the mechanisms and the mechanics of impact, in order to predict the residual strength of the damaged structures.

The earliest observable damage affecting a laminate subject to low velocity impact is typically delamination, which is mainly responsible for the compression strength degradation. Intralaminar fractures, the first failure caused by an impact, have a negligible influence on the mechanical behaviour of the laminate, but they cannot be disregarded since delamination starts from them. For this reason, significant research [20, 22–24] has been devoted to studying the mechanisms of delamination initiation and growth. Since residual material properties after impact are of primary concern in applying damage tolerance concepts, many authors have tried to correlate, analytically or experimentally, the residual strength to impact energy with the damage mechanisms. Most of the previous endeavours have focused on understanding whether the structure could continue to function after an impact, which requires the study of how delamination extension influences the residual capability to support structural loads. Toward this end, it is critical to study the onset, extension, and propagation of delamination in composite laminates subject to low velocity impact. Such an analysis could be carried out by varying the thickness of the laminates and modulating the impact energy up to penetration.

Studies on delamination and other damage mechanisms have often been conducted separately [20–24]. A composite laminate could develop more than one delamination along the thickness during impact, depending on the impact energy and the stacking sequence. How do these delaminations start? How do they propagate? Does one delamination play a stronger role than others during subsequent impacts or transverse loading? Are there interactions between different forms of damage? Answering these questions call for new experimental research that could inform the comprehension of these complex phenomena, verify semi-empirical models, and support the refinement of physically-based theories.

This chapter reports low velocity impact tests up to complete penetration for increasing energy levels, carried out in a modular falling weight tower and followed by non-destructive and destructive damage investigations. Through extensive experiments at increasing impact energies, we sought to investigate damage onset and

propagation, as well as the interaction between several damages. Semi-empirical models for the prediction of the influence of impact parameters on the dynamic behaviour, from the technical literature, were critically examined and verified in the present research. Impact parameters [25, 26], including penetration and absorbed energy, maximum force, indentation depths and delaminated area, were analyzed and utilized to validate the models toward the final aim of predicting the residual strength after impact.

Experiments were carried out on carbon fiber laminates, subjected to experimental low velocity impact tests at three different temperatures: room (or ambient) temperature, −25 °C, and −50 °C. Compression-after-impact (CAI) tests were performed to characterize the residual strength through a new, simpler, apparatus, which was designed and realized at the University of Naples. Ultra sound (US) technique is used to investigate the delamination, and a new holographic technique, ESPI (electronic speckle pattern interferometry), is proposed as a promising alternative technique to gather real time in situ measurements. Measurements were compared with results from US [17–19].

The rest of the chapter is organized as follows. First, we summarize low velocity impact tests on composite laminates until penetration and for different impact energies. Then, we study the influence of impact parameters and the temperature on the impact behavior. Third, we examine the influence of surrounding water on the impact response. Fourth, we report on CAI tests, carried out using the new equipment designed and realized at University of Naples to estimate and predict the residual strength of the impacted laminates. Fifth, we document damage investigations, comparing among the innovative technique ESPI with and traditional non-destructive testing methods. Then, we turn to semi-empirical and analytical models to predict the dynamic response of composites. Finally, we summarize ongoing theoretical research toward an improved understanding of fluid-structure interactions during impact.

## 2 Materials and Experiment

### *2.1 Materials*

We studied carbon fiber reinforced plastics laminates (CFRP), obtained by overlapping $n = 7$, 10, and 13 T700 carbon fabric plies (0°/90°) 300 g/m$^2$, with $t = 2$, 3 and 4 mm nominal thickness. The number of layers was experimentally varied to examine its role on the impact response. Square panels, 600 × 600mm, were fabricated at the Naval Surface Warfare Center (NSWC), by vacuum infusion process using the Ashland Derakane 510A vinyl ester resin, commonly used by the US Navy. The final volumetric fiber percentage, $V_f$, was 48%. From the panels, we cut rectangular specimens 100 × 150mm with a diamond saw, following the ASTMD7137 Standards for CAI tests.

## 2.2 Experimental Setup

Experimental tests were carried out in a drop weight machine, Ceast/Instron, where rectangular specimens were impacted at their geometric center by an instrumented impactor of cylindrical shape, with an hemispherical nose 19.8 mm in diameter. The minimum mass of the impactor was 3.6 kg, but additional weights could be added up to 10.6 kg to increase the impact energy. The maximum drop height of the testing machine is 1 m, which corresponds to a maximum impact energy of 35.7 J with the minimum mass of the impactor. Different impact energy values could be obtained using additional weights and/or varying the drop height. A maximum velocity of 20 m/s could be reached by using a preloaded spring. An impact velocity of about 4.0 m/s was measured for the tests reported below.

The drop weight apparatus was equipped with a motorized lifting track. A piezoelectric load cell allowed to record the force–time curve. The acceleration history was calculated by dividing the force by the mass of the impactor. The displacement curve was obtained by double integration of the acceleration, and the force–displacement curves were plotted. At the initial time, the dart coordinate is zero and its initial velocity can be obtained from standard dynamics [24, 25], as follows:

$$\nu_0 = \sqrt{2g\Delta h} \tag{1}$$

where $\Delta h$ is the height loss of the center of the mass of the dart, with respect to the reference surface of the specimen and $g$ is the gravity [24, 25]. The impact velocity was also measured by an optoelectronic device.

Data were stored after each impact and the impactor was caught by an anti-rebound system to avoid multiple impact on the same specimen. The specimens were loaded until complete penetration; the whole load-displacement curve, up to penetration, is offers important insight into the impact in terms of the relationship between the force and the deflection of the panel. Characteristics points on the rising path of the load curve, such as load drops or local changes in slope, were used to evidence variations in material behavior as a consequence of a damage. Measurements were carried out at increasing energy levels and followed by indentation tests to investigate the damage onset and propagation.

During each test, the complete force-time and force-displacement curves, as well as energy and velocity curves, were recorded by the DAS16000 acquisition program and successively studied to evaluate the impact parameters (maximum force and corresponding displacement, absorbed energy, and failure load). All the parameters obtained in different conditions were compared. We tested three different energy values, 5 J, 10 J and 20 J, to study damage formation and propagation.

Updating the machine with a thermal chamber allowed to perform tests at low temperatures, up to −50 °C. Liquid Nitrogen was used to lower the temperature. From 10 to 15 min were necessary to measure −25 °C and −50 °C in the chamber, before each single test could be conducted. The specimens were stored in a freezer at

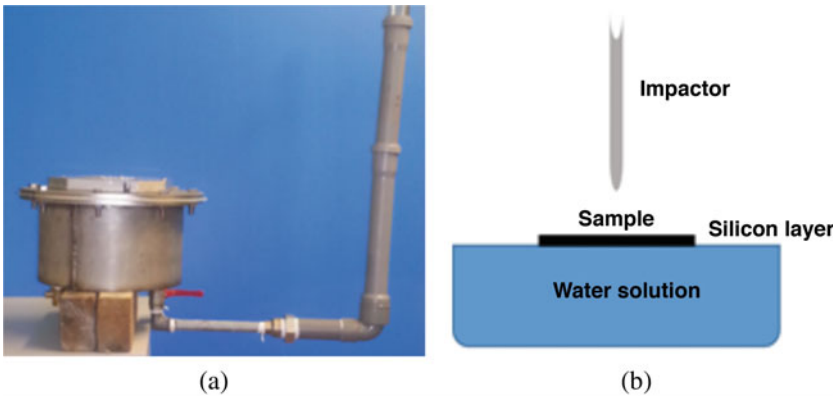


**Fig. 1** (**a**) Steel box full of water and (**b**) schematic view of the experiment

−18 °C for 14 h. When the thermal chamber reached the desired temperature for the test, the samples were installed on the support and were kept into the conditioned chamber until they reached the test temperature (−25 °C or −50 °C). The temperature of the specimens was monitored by a thermocouple. Traditional air-backed loading tests were first carried out at room and at the low temperatures of −25 °C and −50 °C. Then, we conducted water-backed loading tests, labeled as "FWB", and tests on samples fully immersed in the water column, labelled as "immersed". Specimens were loaded at the same impact energies and temperatures, reproducing air-backed impact conditions. The aim of this comparative study was to study the influence of the water on the response of the composite due fluid-structure interaction.

In Fig. 1a, the equipment used for FWB tests is shown, while Fig. 1b sketches the proposed experimental scheme. The latter has been proposed by the University of Naples, where the setup is based on a modified drop weight machine, in which an instrumented impactor falls on a clamped specimen which rests upon a water column to obtain a load distribution on the entire surface of the specimen. Specifically, a novel experimental framework was designed to elucidate the impact response of water-backed marine laminates at varying temperatures. The setup is constituted by an instrumented water-filled box used as a support, where panels are first simply supported and then fully clamped and subjected to low velocity impact in a drop tower. During the impact, the deformation of the panel, the motion of the impactor and the pressure field in the box are recorded to ascertain the severity of the impact and quantify fluid-structure interaction.

To avoid water splashing during the impact, a thin silicone deformable bag was used for covering the water solution contained in a cylindrical rigid steel box, 200 mm in diameter (Fig. 2a), and the specimen was positioned on the water pillow. A circular steel plate, 8 mm in thickness, with a rectangular window of 100 × 150mm to house the specimen, was bolted on the box container (Fig. 2b). The specimens were simply supported by the water layer to simulate free boundary

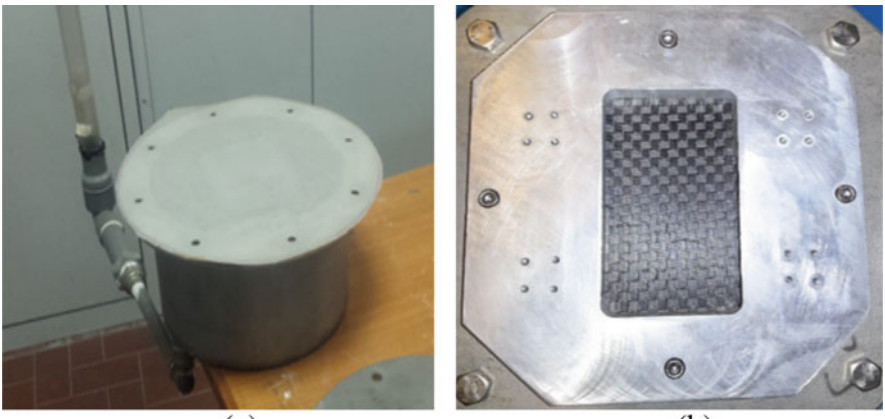


**Fig. 2** (**a**) Silicon layer to avoid the leakage of water and (**b**) frame on the steel cover for the specimen positioning

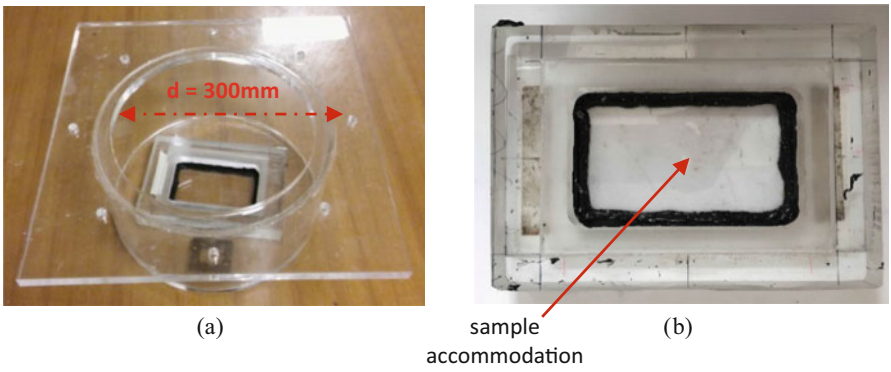


**Fig. 3** (**a**) Experimental set up: plexiglass tank containing water (**b**) and detail of the support. Reproduced form [40]

conditions and facilitate a precise assessment of the material response of the panels, in the presence of water backing. The box was filled with a quantity of water greater than the one necessary to reach the edges, to create a water pillow beneath the specimen, minimize any resistance of the sheath during the impact, and allow contact of the entire back surface of the panel. The specimens were impacted on their free side by the cylindrical impactor described above. Specifically, the setup facilitates in diffusing the concentrated loading of the impact to a distributed dynamic loading along the whole wetted surface. To avoid ice formation at $T = -25\ ^{\circ}\mathrm{C}$ and $-50\ ^{\circ}\mathrm{C}$, an antifreeze liquid with a density similar to the water, was added to the water.

Tests on specimens immersed in the water (Fig. 3a) were performed in a plexiglass tank, 300 mm in diameter. In these tests, the laminates were impacted

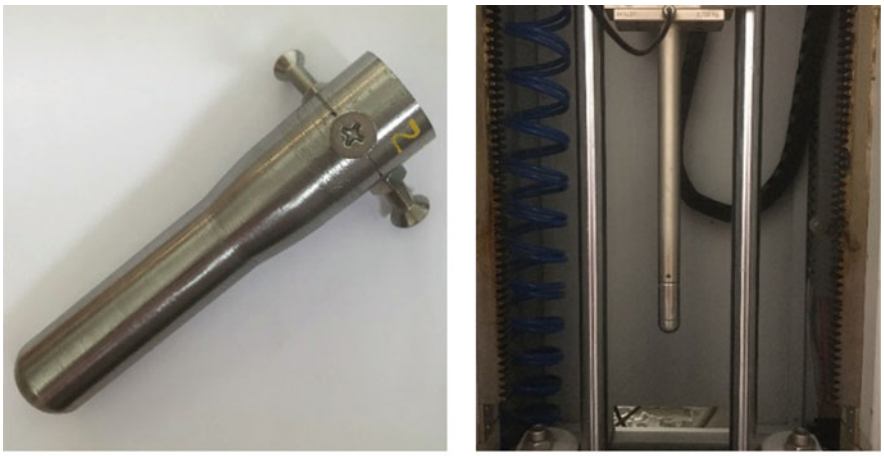


**Fig. 4** (**a**) Impactor modified for the in-water tests (**b**) and impactor suggested by the Standard

from the water side. Figure 3b shows the plexiglass support, which was machined to reproduce the one suggested by the ASTMD 7137 standard with an internal rectangular window 75 × 150 $mm^2$ to house a specimen. The support was entirely immersed in the water and fixed on the bottom of the tank. A thin polymeric layer was sealed on the support to avoid water on the back of the specimen.

It was necessary to modify the impactor of the Ceast/Instron impact machine for loading the specimens on the bottom of the tank. Specifically, a longer blunt with the same hemispherical nose (Fig. 4a) was glued and fixed by screws on the first original body (Fig. 4b). Although the longer arm, along with the glue and the screws, caused significant measurement noise in the force signals, the general trend was not affected.

A schematic view of the clamping device suggested by the ASTMD7137 Standard is reported in Fig. 5. To exactly reproduce the same boundary conditions during the water backed tests, a rectangular frame of 75 mm by 125 mm (Fig. 6a) was machined on the steel plate to cover the steel tank containing water shown in Fig. 2. Four black rubbers (Fig. 6b) were used to clamp the specimen at four points, similar to traditional impact tests in air. The latter tests will be labelled as WB to distinguish them from the ones labelled as FWB where the specimens were merely supported by the water pillow.

All the parameters obtained in the different conditions were compared. The use of three impact energies, 5 J, 10 J and 20 J, allowed for the study of the damage onset and propagation.

The indentation depths, *I*, (the plastic deformation produced by the indenter on the material/impactor contact point during the impacts) were measured using a confocal microscope, LEICA DCM3D. This advanced apparatus allows for acquiring three-dimensional images of the sample, thereby extracting salient information about the profile and the depth of the indentation from the three-dimensional shape

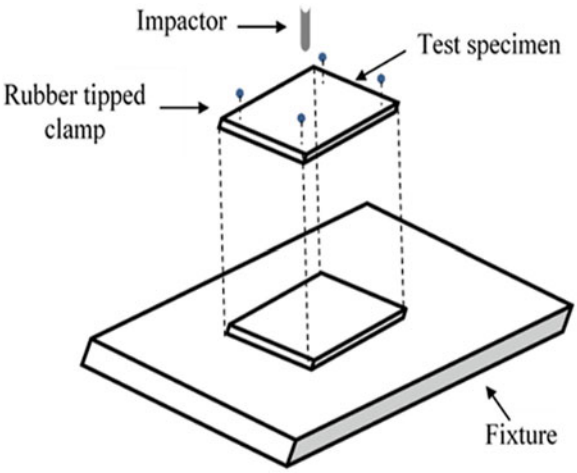


**Fig. 5** Clamping device from ASTMD7137 standard. Reproduced form [40]

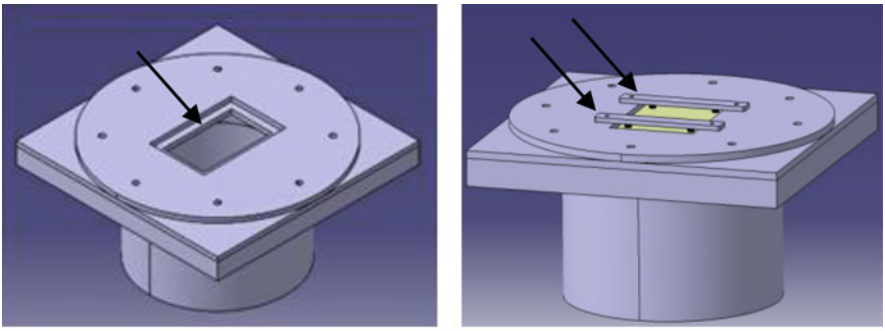


**Fig. 6** Rectangular frame 75mm × 125mm (**a**); clamping device (**b**). Reproduced form [40]

of the surface. A dedicated software was used to acquire and manage the indentation data, obtaining the shape and roughness values according to the international standard (ISO 4287).

The microscope is equipped with an x-y table and different magnifications, from 5x up to 150x. In Fig. 7, an example of acquisition of an impacted surface is reported. From the picture, we can appreciate the ability to clearly resolve the indentation (dark blue area) as well as the precision of surface reconstruction.

The ultra sound technique by the Olympus OmniScan® SX Phased Array Probe, 5 MHz Linear Array (automated data acquisition system with a16:64PR phased array unit) was used to characterize the internal damage [27]. The pulse echo technique [28] was adopted to detect the depth of the delaminated area, such that the damage was identified by the echo signals (first echo, back-wall echo and defect echo) captured by the probe. The coupling agent was a layer of water and contact sound testing was performed.

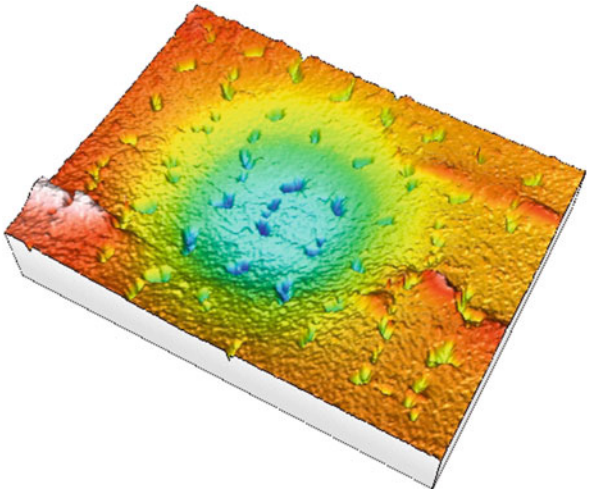

**Fig. 7** Example of surface image recorded by the confocal microscope after the impact test at 10 J

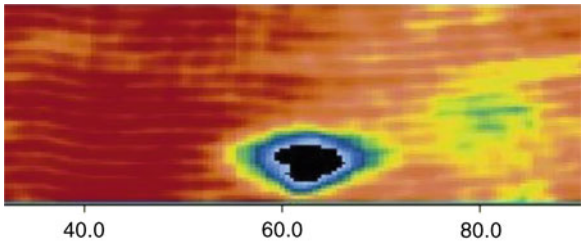


**Fig. 8** Example of damage detected by ultra sound

Through C-scan inspection, we obtained a plane view of the damage, from which the software yielded the entire plane image of damage induced by the impact. The acquisition system was calibrated using an undamaged sample. The latter was found to be associated with a uniform color (usually dark red), while damaged areas are usually represented by different colours (Fig. 8) as a function of the severity of the damage. In this way, the damaged area was easily identified and measured. Longitudinal and transverse damage dimensions were recorded using M2M software, whereas each delaminated area was imported in a CAD software, bordered and measured. The acquisition system was calibrated using an undamaged sample by following a procedure standard practice in the aeronautical field.

Internal damage was also investigated via a speckle technique (ESPI). This technique allows us to measure the out-of-plane displacements of a stressed specimen, for identification of strains, along with cracks on rough surfaces with high sensitivity and in real time, without any physical contact [27, 29]. ESPI belongs to the family of coherent light interferometry techniques that includes holographic interferometry and shearography [26]. The detection of invisible and barely visible micro-deformations and micro-cracks is possible by scanning the surface by a laser, at wavelength of 532 nm, and the measurement accuracy is related to the wavelength.

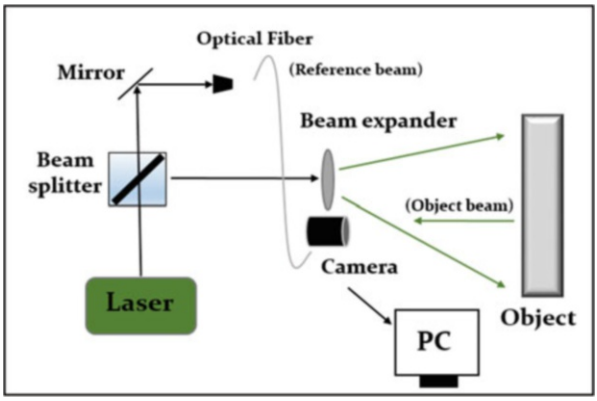


**Fig. 9** Basic scheme for the ESPI system

A CCD/CMOS camera records the deformation in the form of correlation fringes, associated with a slight temperature increase in the material due to damage. A basic scheme of the system for recording speckle interferometry measurements is illustrated in Fig. 9. The laser beam is split into a reference beam and an object beam by means of a splitter, which enables control of the relationship between the reference and the object. A speckled image of the object, resulting from the interference between the wavefronts of the two beams on the plane of sensor camera, is recorded. When the specimens are deformed due to an external perturbation, thermal or mechanical, the wavefront reflected from it is slightly changed, while the wavefront from the reference beam does not change.

A speckle pattern is recorded by the camera and stored by a computer. The subtraction of the speckle patterns registered for the deformed and non-deformed conditions provides the correlation fringes. When the subtraction is computer-aided, the technique is called electronic speckle pattern interferometry. The correlation fringes are also digitally treated to remove undesired noise and enhance contrast in phase-contrast maps (Fig. 10a). From the latter, it is possible to quantitatively measure the displacement field with high accuracy. The measured displacement is "out of plane" due to the geometrical configuration of the laser illumination. Figure 10 illustrates correlation fringes acquired by a CCD camera, the unwrapped phase-contrast map, and a magnification of damaged area with the estimation of the delaminated area.

All the data collected during the tests were used to validate existing semi-empirical models for the prediction of the dynamic behaviour of composite laminates.

After the impact tests, the specimens were tested in compression, CAI, to investigate their residual compression strength after loading. The residual properties of the laminates after dynamic loading are of crucial importance to assess whether the damaged structure should be replaced or could continue to support mechanical loading. Due to the practical ramifications of this information and the complexity of existing equipment suggested by the Standard ASTM D7137, the Department of Chemical, Materials and Industrial Production Engineering of University of Naples

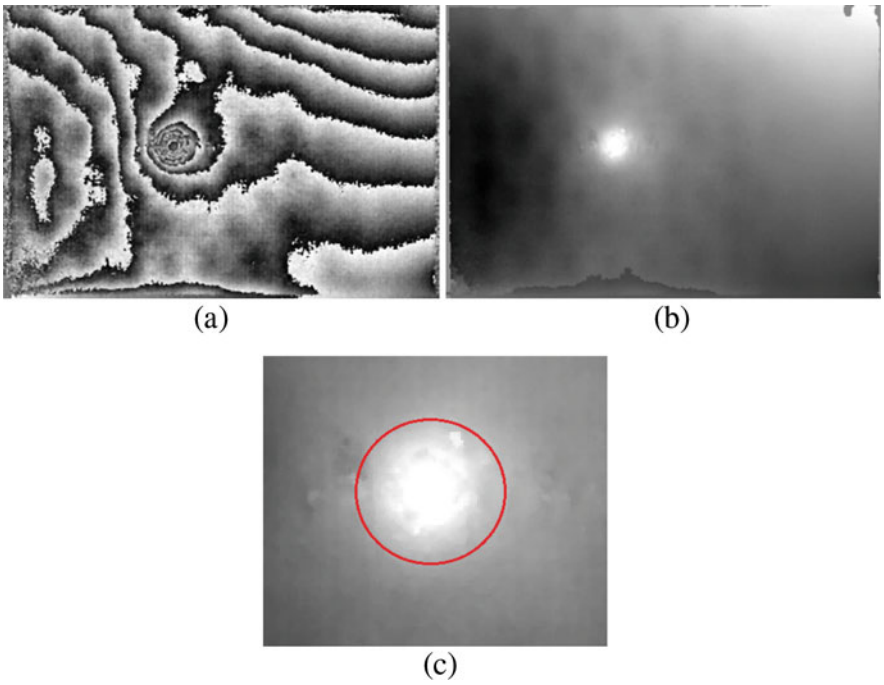


**Fig. 10** (**a**) Correlation fringes (**b**) unwrapped phase-contrast map (**c**) and magnification of damaged area and the estimation of delamination

conceived a new, improved equipment that mitigates the problems of buckling and misalignment of the specimen with respect to the load. These latter phenomena often result into extended time for testing and, consequently, higher costs. The new equipment allows for the acquisition of more reliable information in a shorter time.

The existing ASTM Standard proposes the application of a compressive load through a fixture for the stabilization of the sample (Fig. 11a), which comprises several different parts, three on the front side and three on the back side, each one disconnected from the main body, (black arrows in Fig. 11b), The lateral two blocks, marked through red arrows in Fig. 4a, are disconnected from the main body, thus requiring fixing them through bolts.

In the design of the new fixture (Fig. 11b), the two lateral wings are part of the same block of the main body, and the number of the bolts to fix the sample is drastically reduced. In this way, a rigid body with a single bolt each side was realized. The sample has to be placed on a single sliding guide (marked as black arrows in Fig. 11b), fixed to the rigid main body through a single bolt on the floor. The guides ensure the alignment of the specimen and the applied load. Moreover, the three different parts are fixed to the main body through guides with a limited number of bolts. Differences and advantages of the new equipment can be readily appreciated by comparing the designs through Fig. 11.

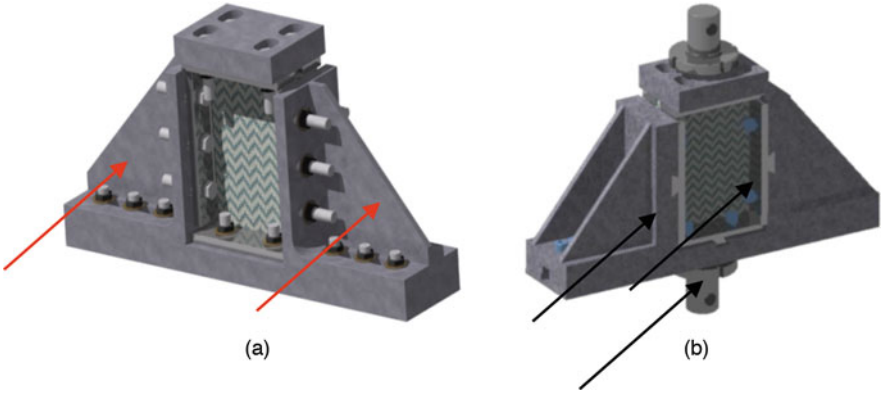


**Fig. 11** (**a**) CAI tests equipment: ASTMD7137 (**b**) and new design at the University of Naples. Reproduced form [41]

**Fig. 12** Failures after CAI tests: (**a**) "correct" and (**b**) "incorrect"

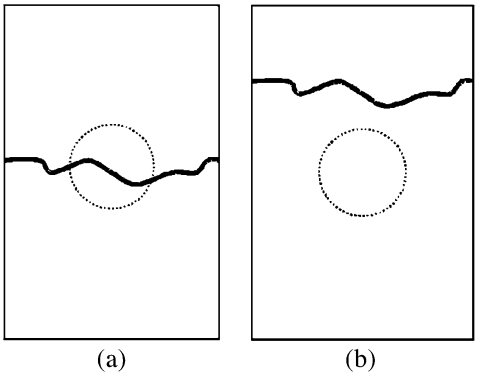


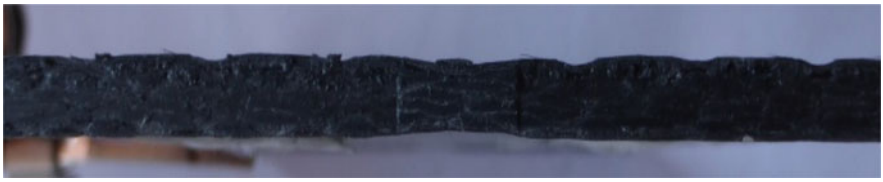

**Fig. 13** Fractographic analysis of the section of the specimen showing defects due to a poor compaction

However, the validity of the tests strongly depends on the ability to attain specimens with parallel lateral sides and on the quality of the laminate. Both these problems could lead to incorrect failures, which will challenge the evaluation of the residual strength. In fact, a correct failure pattern should cross the impacted damage area at the central point (Fig. 12). Nonparallel lateral sides and defects could lead to a local concentration of the load on the upper side, thereby triggering localized failure (Fig. 13).

Four strain gauges, two on the front and two on the back side, were glued on each specimen following the suggestions by the Standard.

## 3 Background: Residual Strength after Impact

In the literature [12–16], the residual strength after low velocity impacts was found to be influenced by the impact energy, U, following the trend in Fig. 14. Three zones are highlighted in the figure, summarizing the response of the laminate at increasing energy levels. In region I, the impact energy is below the threshold value for the damage initiation; in region II, the residual strength quickly reduces to a minimum; and in region III, we observe constant trend since the perforation has occurred.

The residual tensile strength is a function of the delaminated area and the size/shape of the impactor, whereas the residual compression strength depends only on the delamination, since it is controlled by local buckling of delaminated plies [16]. Moreover, delamination can be caused by low impact energy, so that, in correspondence of about 0.3 mm of indentation depth, large strength reduction might occur [17].

A linear elastic fracture mechanics model to predict residual strength as a function of kinetic-energy, was proposed in [12], yielding adequate correlation to experimental results:

$$\frac{\sigma_r}{\sigma_0} = \left(\frac{U_0}{U}\right)^{\alpha} \tag{2}$$

where $U_o$ and $\alpha$ are two experimental constants and so is the strength of the non-damaged material.

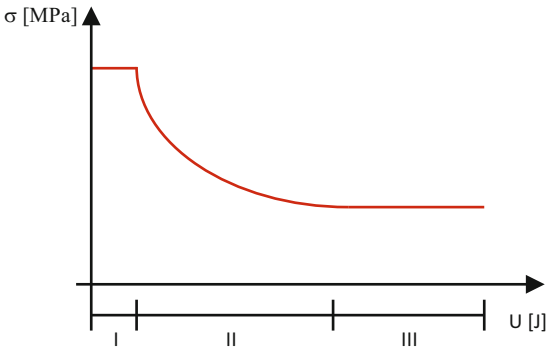


**Fig. 14** Trend of the residual strength after impact, as a function of the impact energy

# 4 Results and Discussion

## *4.1 Non Destructive Damage Investigation*

In Fig. 15, we compare results obtained on equivalent carbon fiber laminates using the two different non-destructive investigations introduced above. Both the US and ESPI techniques are able to capture the delamination and, more importantly, to clearly highlight the lobe shape, which is typical of the delamination between differently oriented layers. This result is particularly promising, whereby it highlights the potential of a technique, ESPI, which is not widely disseminated in the composites community, to investigate their internal damage.

In Fig. 16, we report the delaminated area against the impact energy to highlight the good agreement between the two techniques. All the data follow a linear trend suggesting that, in the studied range of impact energies, as the energy, U, increases, the internal damage, A, increases accordingly. It is worth to note that the intercept with the horizontal axis represents a threshold limit of the impact energy necessary for the delamination onset and below which no delamination is measured between the layers. This aspect will be hereafter discussed again.

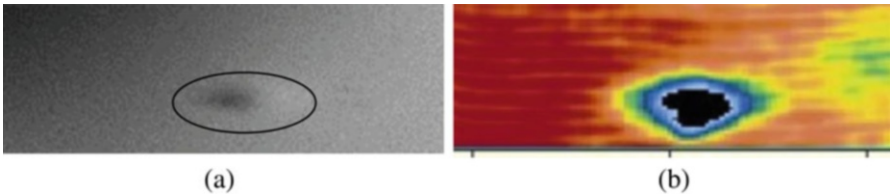


**Fig. 15** (**a**) Non-destructive damage quantification on the backside, for an impact of 13 J: holography (**b**) and ultra sound

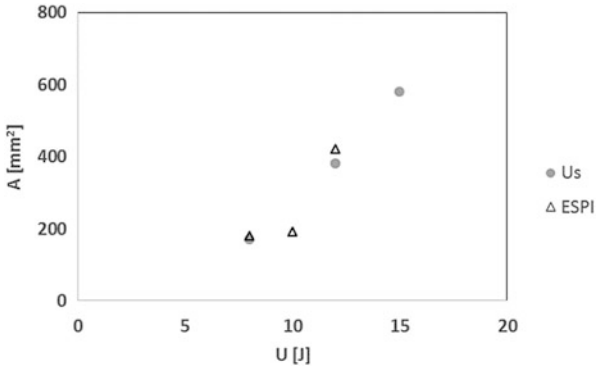


**Fig. 16** Delaminated area, *A*, vs impact energy, *U*, quantified using two non-destructive techniques

## 4.2 Semi-empirical Models: Influence of the Temperature

Semi-empirical models available from literature were systematically validated against the collected experimental data. The load-displacement curve at penetration, recorded during each experimental test, offers salient information about behavior of the material [30], in terms of material properties and damage mechanisms, while allowing for comparing responses from different loading conditions, such as those at room and low temperatures (Fig. 17). It displays some features that are common to all laminates, despite differences in thickness, architecture, and physical properties, affording the opportunity to identify key parameters.

From the shape of the curve it was possible to gather information about: (a) the first damage, usually delamination, which was evidenced by the first load drop or change in the slope along the rising part of the curve; (b) the first failure load, which is the load that caused the first damage; (c) the energy, measured as the area under the curve up to the first failure load; (d) other damages, such as fiber failures, from load drops near to the maximum load; (e) the absorbed energy; and (f) the penetration energy. A load drop or a change in the slope on the rising part of the curve reflects a change in the structural rigidity of the material and could be utilized as an effective parameter to reveal damage initiation and propagation.

Decreasing the temperature was found to affect the load curves, thereby supporting the influence of temperature on the dynamic response of the laminates. By comparing the curves (Fig. 17a), it was found that its effect is similar to increasing the thickness of the laminate (Fig. 17b), whereby we registered an increase in the maximum force, rigidity, and penetration energy.

The higher penetration energy and maximum load at low temperatures could be explained by the brittle mechanism of damage formation [31], which promote the formation of a large number of cracks in the matrix. At room temperature, the energy associated with the formation of these cracks is, instead, absorbed for elastic and plastic deformation. Brittle behavior at low temperature was confirmed in [32] in terms of lower measured indentation depths, where the indentation represents the

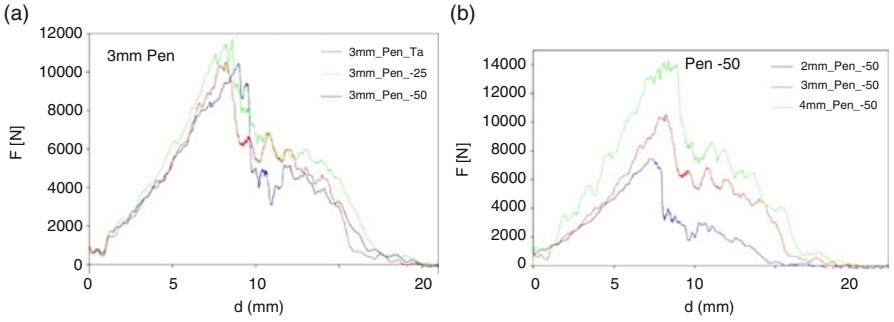


**Fig. 17** (**a**) Force displacement curves at penetration for carbon fiber laminates: $n = 10$ (**b**) and $n = 7$, 10 and 13. Reproduced form [9]

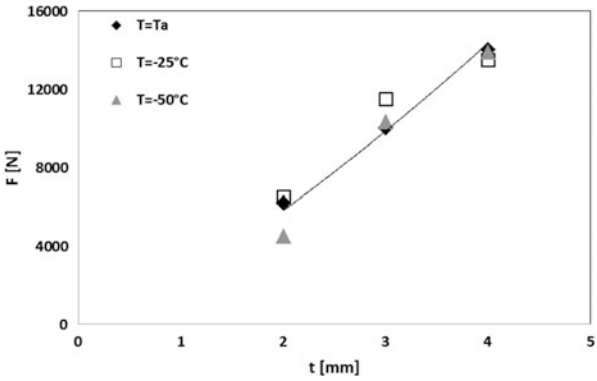


**Fig. 18** Hertzian contact law validation for different temperatures

plastic deformation of the surface of the laminate due to the impactor-material contact point. Unfortunately, it was not possible to perform the same analysis on CFRP laminates of naval use studied since no indentation was measured on them. The latter was probably due to the large fiber bundles of the carbon fabrics.

The maximum load, $F_{max}$, inferred from the load-displacement curves, was plotted against the thickness, t, for the different testing temperatures (Fig. 18) to validate the Hertzian contact law for the prediction of $F_{max}$. Such a correlation might offer imporant insight into the influence of the thickness on the load which causes internal damage [30], that is,

$$F_{\max} = a \cdot t^m \tag{3}$$

where $a$ and $m$ are two experimental constants, which we identified as $a =$ 2.36 N/mm^$m$ and $m = 1.3$. From Fig. 18, we can appreciate the increase in the maximum load with decreasing temperatures; therein we use a subcript "a" to identify ambient temperature and a consistent notation is maintained throughout the chapter.

The same analysis was pursued in [33] to predict the first failure load. However, the most significant load drop was found in correspondence with the maximum force such that damage which occurs before would not significantly affect the curve.

The effect of temperature on the penetration energy, measured as the area under the complete load-displacement curve, was also studied. We found that higher energies are necessary to penetrate the same laminates for lower temperature, and, as expected, the penetration energy increases with the number of layers. We plotted the penetration energy, $U_p$, against the compound quantity $t{\cdot}V_f{\cdot}D_p$, (Fig. 19), where $t$ is the thickness, $V_f$ the fiber volume fraction, and $D_p$ the diameter of the impactor. In agreement [24], we discovered a power law which is useful to predict $U_p$ from known experimental quantities. Specifically, we found

$$U_p = \alpha \cdot \left(t \cdot D_p \cdot V_f\right)^{\beta} \tag{4}$$

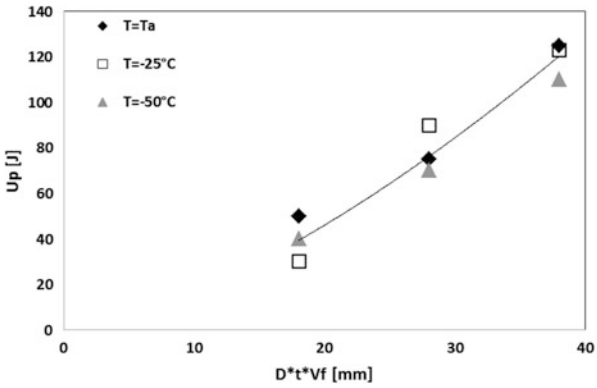


**Fig. 19** Penetration energy against the compound quantity $t \cdot V_f \cdot D_p$, for different temperatures

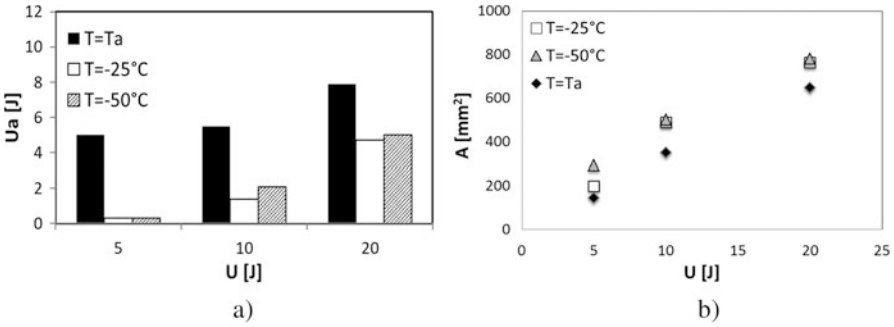


**Fig. 20** Influence of the temperature on (**a**) absorbed energy and (**b**) delamination area for laminates of 3 mm in thickness

where $\alpha = 0.87$ J/mm and $\beta = 1.34$ are two constants that were experimentally determined, irrespective of the temperature. In particular, $\alpha$ depends on the material and $\beta$ on the phenomenon being independent of the material.

This semi-empirical model highlights the importance of the fiber content in an impact phenomenon and it allows us to compare data obtained on different material systems and test conditions, as seen by its validity in extreme temperature conditions. Moreover, this model allows to predict the penetration energy as a function of the impactor diameter. Since the penetration energy is related to the residual strength through the indentation [34], one may estimate the residual strength from a simple indentation measurement.

The absorbed energy represents a crucial parameter in dynamic phenomena. It is the energy necessary to create damage and propagate it. Understanding the mechanisms of energy absorption requires elucidating damage onset and propagation, as well as damage interaction during the loading phase.

By inspecting Fig. 20a, which shows the influence of temperature on absorbed energy for a fixed impact energy, we gather that the absorbed energy decreases for

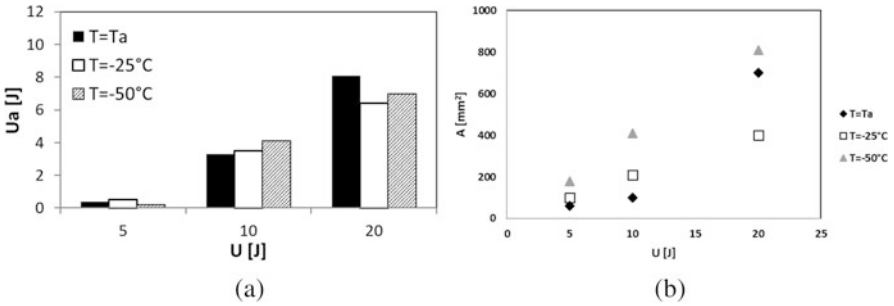


**Fig. 21** Influence of the temperature on (**a**) absorbed energy and (**b**) delamination area for laminates of 4 mm in thickness

lower temperature. Thus, at low temperatures, it is easier to initiate and propagate internal damage. The influence of the impact energy on the delaminated area, $A$, was studied at low temperature as shown in Fig. 20b. In correspondence to a decrease in the temperature, an increase in the internal damage extension was registered. This effect is more evident at larger impact energies. Overall, this finding is in line with the experiments that suggest that less energy is absorbed at low temperature [35], due to the ease of damage propagation, as confirmed in Fig. 20a.

Moreover, the delaminated area was found to increase with the impact energy, but the trend seems to become more linear at lower temperatures (Fig. 20b). While at room temperature the damage of laminates of 3 mm in thickness becomes constant after a certain impact energy value, it continues to increase at temperatures less than 0 °C, indicating the onset of more severe damage mechanisms.

A different behavior was observed for laminates of 4 mm in thickness (Fig. 21). Significant differences on the absorbed energy were noted for an impact of 20 J, thereby highlighting the role of rigidity in the dynamic response of laminates [30]. The larger delamination at low temperatures explains the lower residual strength reported and commented hereafter in Figs. 23 and 25.

The extension of the delamination with the increase in the thickness is larger also at low temperatures, confirming the difference between the bending effect, predominant in thinner laminates, and the shear one, usually affecting the response of thick laminates, as extensively discussed in the literature and by the authors in [30].

Prompted by the open debate about the relative importance of impact energy and maximum force on the delamination extension [36, 37], we identified a linear trend between the delaminated area and the maximum load, $F_{max}$, irrespective of the thickness. All the experimental data from Fig. 20, follow a single linear trend, irrespective of the testing temperature (Fig. 22). Therefore, we identify threshold values for the delamination initiation, below which no delamination should take place in the laminate.

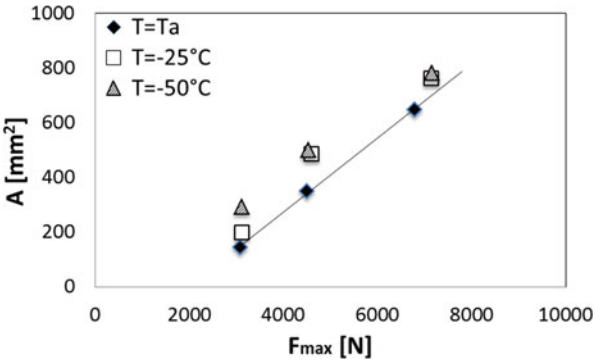


**Fig. 22** Delaminated area, A, against the maximum load, $F_{max}$. Data from Fig. 20

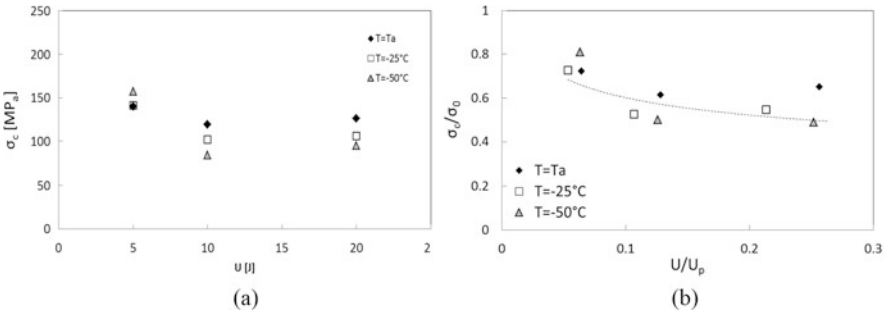


**Fig. 23** Residual strength of a laminate of 3 mm in thickness (**a**) influence of impact energy (**b**) and semi-empirical model in Eq. (2)

## *4.3 Residual Strength: Air-Backed Tests*

The trend found in literature [12] regarding the dependence of the residual strength on the impact energy was confirmed at low temperatures. Specifically, Fig. 23a illustrates such a trend for carbon laminates of 3 mm in thickness. A perceptible decrease of the residual strength at decreased temperature is noted, except when the specimens were impacted at a level of 5 J in energy. In that case, we registered similar values between room temperature, −25 °C and higher values at −50 °C.

In Fig. 23b, the power law in Eq. (2) is verified using data from Fig. 23a for an exponent $\alpha = 0.25$. This important relationship between the residual strength and the impact energy should afford the prediction of the residual properties of a composite laminate that is dynamically loaded.

Differently from [3], plotting the residual strength against the delaminated area (Fig. 24), we observed the same decreasing trend reported in Fig. 23, with, perhaps, a horizontal asymptote. Such a trend is justified by the linear increase of the delaminated area for increasing impact energy, as shown above.

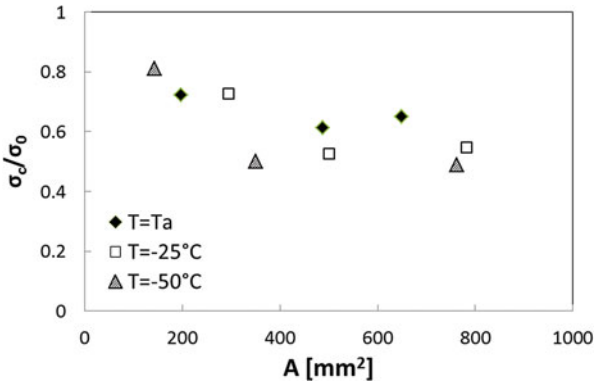


**Fig. 24** Non-dimensional residual strength versus delaminated area for laminates of 3 mm in thickness

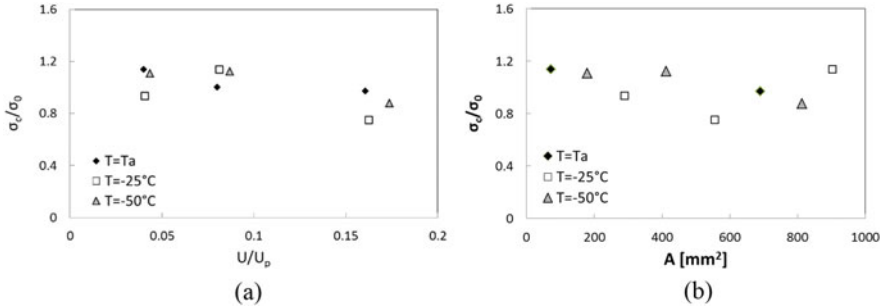


**Fig. 25** Residual strength of a laminate of 4 mm in thickness (**a**) influence of impact energy (**b**) and semi-empirical model in Eq. (2)

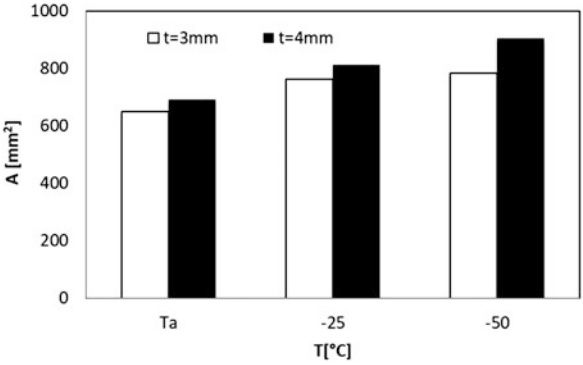


**Fig. 26** Influence of the thickness on the delaminated area at different temperature

An equivalent analysis was performed on the 4 mm-thickness laminate as shown in Fig. 25. Therein, we observe a flatter trend for the residual strength as a function of impact energy, compared to the delamination analysis. This suggests a lower residual strength reduction, along with a weaker influence of the temperature for composites of higher thicknesses. Such an observation is confirmed by the lower internal damage measured in these conditions (Fig. 26).

At room temperature, increasing the thickness of the laminate results leads to an increase in the stiffness, whereby most of the absorbed energy is utilized to create internal damage that causes lather delamination. In contrast, for thinner laminates, bending allows for a larger energy absorption, thereby hampering delamination [30].

## *4.4 Residual Strength: Water-Backed Impact Tests*

Low velocity impact tests on free water-backed samples were carried out at the same impact energies as in-air tests. In Fig. 27, the load-displacement curves obtained by impacting the specimens of 4 mm in thickness at 20 J are compared. Predictably, the shape of the curves is different as well as the maximum load and displacement experienced by the laminate.

In contrast with one's intuition, the maximum load and initial rigidity are higher in the absence of the water. This is attributed to the different boundary conditions employed in the tests, whereby water-backed panel are suspended above a water pillow that might, in principle, allow for rigid-body motion of the sample. In contrast, specimens tested in air are fixed on their sides, causing a higher resistance to the impact.

In Fig. 28, we compare the delaminated area for in-air and free water-backed impact, which confirms that the specimens are subjected to more severe loading conditions when tested in air.

Because of the lower delamination, we also register (Fig. 29) higher residual properties for water-backed specimens, except for the case of laminates of 4 mm thickness that were impacted at 10 J.

These anomalous results prompted a collaboration with Prof. Porfiri's group, who is honing a physically-based mathematical model to examine the dynamic response of water-backed panels that takes into account the elastic response of the composite at moderately-large deformations, the role of the boundary conditions, and the added mass effects from the fluid-structure interactions. The theoretical underpinnings of the model are presented later in the chapter, along with some preliminary results on homogenous, isotropic panels.

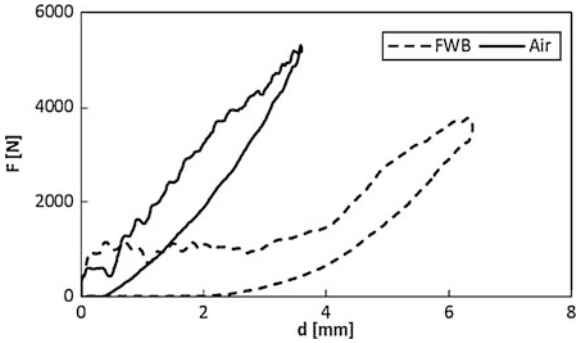


**Fig. 27** Load-displacement curves comparison for laminates of 4 mm in thickness impacted at an energy of 20 J

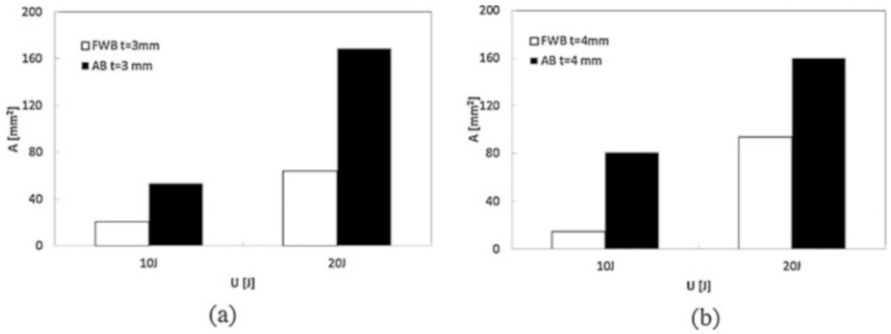


**Fig. 28** Delamination measured in air and free water-backed tests: (**a**) $t = 3$ mm (**b**) and $t = 4$ mm

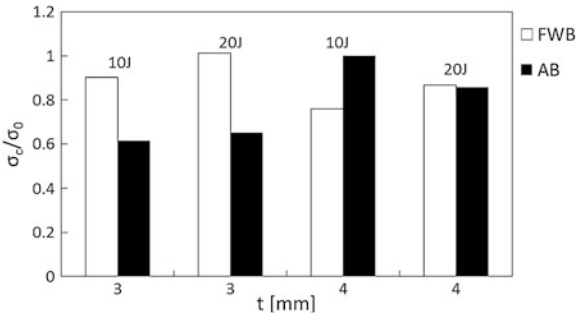


**Fig. 29** Residual strength: comparison between pure impact in air and free water-backed tests

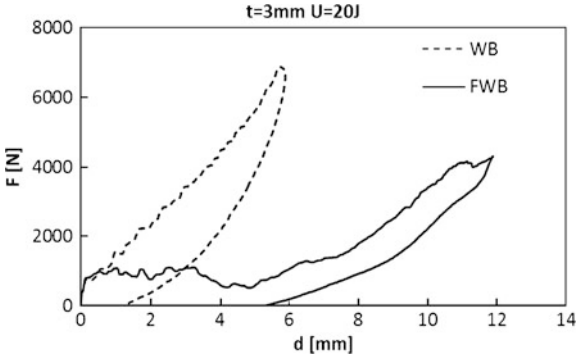


**Fig. 30** Clamped water-backed and water-backed free: comparison between load curves for laminates of 3 mm in thickness, impacted at 20 J

## *4.5 Effect of the Clamping Device and Fluid-Material Interaction*

In Fig. 30, load curves obtained in free water-backed and clamped water-backed impact tests are compared to ascertain the critical role played by the boundary conditions. The initial stiffness and maximum load experienced by clamped specimens is considerably higher than those that were merely supported by the water column.

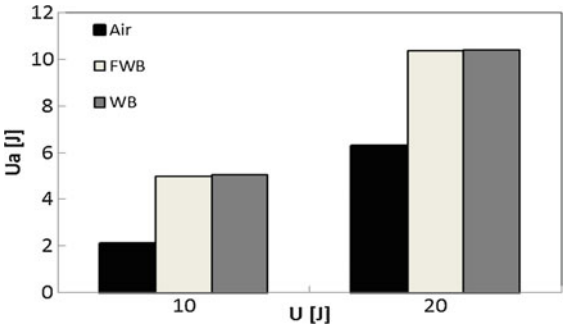


**Fig. 31** Absorbed energy versus impact energy for laminates of 3 mm in thickness

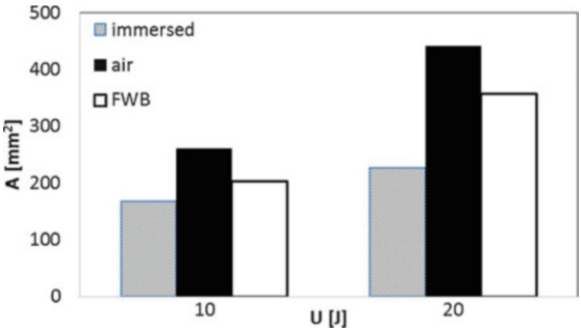


**Fig. 32** Delamination versus impact energy for laminates of 3 mm in thickness

Notwithstanding these differences, the energy absorption between the two conditions is quite similar (Fig. 31), potentially pointing as a local failure process that is marginally affected by boundary conditions. Comparing both the water-backing setups with in-air impact, we confirm an increase in the absorbed energy, which might be associated with the added mass effect from the motion of the surrounding water.

Even if the absorbed energy is higher when the panel is in contact with water (Fig. 31), Fig. 32 shows that the delamination propagates more in experiments in air. This phenomenon could be again explained by the added mass of the water, which causes a redistribution of the load that is ultimately diffused throughout the extent of the panel.

## *4.6 Impact on Specimen Immersed in the Water*

To simulate more closely impact conditions of marine composites, impact tests were performed on specimens fully immersed in the water. In this condition, the sample was at the bottom of a water tank, with its wet side being impacted. By comparing the results obtained in this case with in-air and water-backed samples, we noted a difference in the absorbed energy and displacement. In Fig. 33, all load curves have

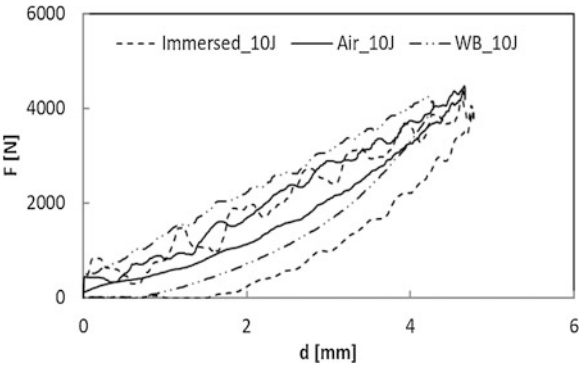


**Fig. 33** Comparison at 10 J between for all testing conditions

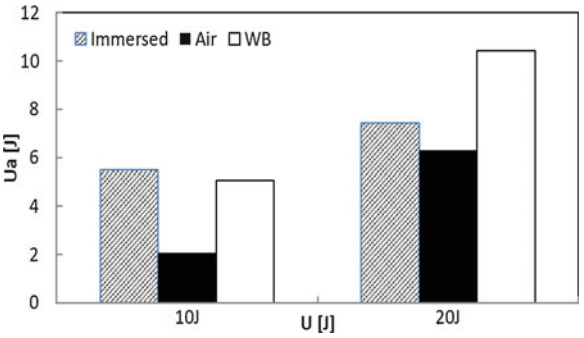


**Fig. 34** Absorbed energies versus impact energy for laminates of 3 mm in thickness

similar shapes, irrespective of the support, showing similar initial rigidity and maximum loads that are very close, whereas different amounts of absorbed energy (Fig. 34) were measured.

The results suggest the presence of multiple mechanisms of damage evolution, represented by the different absorbed energy in the presence of the water. An interesting consideration can be offered by looking at Fig. 34. The lower energy of 10 J results in a higher absorbed energy when the panel is immersed in the water, even if energy absorption between water-backed and fully immersed samples are very close to each other. On the other hand, in-air panels present the lowest values of energy absorption. Increasing the impact energy to 20 J, in-air samples continue to absorb the least amount of energy, but we observe a significant difference between water-backed and immersed samples, with the former absorbing more energy. It is difficult to explain the difference between the response of WB and immersed samples. However, it is likely that the fluid-structure plays a major role. Ongoing work on mathematical modelling will hopefully be able to address this aspect.

## 4.7 Introduction to the Theory

A physically-principled understanding of the fluid-structure interaction occurring during the impact is currently not available. To fill this gap in knowledge, we developed a reduced-order modeling framework of water-backed impact, focusing on in-plane deformation of thin panels. We specifically analyzed the dynamic response of a beam resting on an infinitely-extended water domain, clamped at both its ends. The beam is loaded at its midspan by a concentrated force, simulating the fall of a heavy mass. The modeling framework is based on nonlinear Euler-Bernoulli beam, to account for nonlinear stiffening due to membrane stretching. Water backing is modeled using potential flow theory with a simplified linear treatment of the boundary conditions inspired by the classical work of Wagner [39]. Based on this premise, we can exactly compute the hydrodynamic pressure on the beam as a function of its acceleration. Hydrodynamic pressure acts as a nonlocal added mass effect, where the local acceleration of the beam will translate in a pressure everywhere on the structure.

The Galerkin discretization is used to transform the governing nonlinear partial integro-differential equation for the deflection field into a mathematically tractable set of nonlinear ordinary differential equations. We established two semi-analytical solutions, by using a polynomial approximation of the in-vacuum linear mode shapes of the beam (assumed modes, AM, method) and Hermitian finite element basis functions (one-dimensional finite element, 1D FE, method). A Newmark-type integration scheme is combined with the modified Newton-Raphson method to predict the dynamic response of the panel.

Results were specialized to plain vinyl ester resins panels and semi-analytical findings validated against full two-dimensional finite element simulations, performed using the commercial software COMSOL Multiphysics. The comparison with such computationally expensive simulations offers compelling evidence for the validity of the mathematically-tractable approach, which is amenable to future generalizations to complex geometries and damage models. Figure 35 illustrates the COMSOL implementation of the problem, clarifying the boundary conditions used in the simulation, along with the mesh used for the analysis.

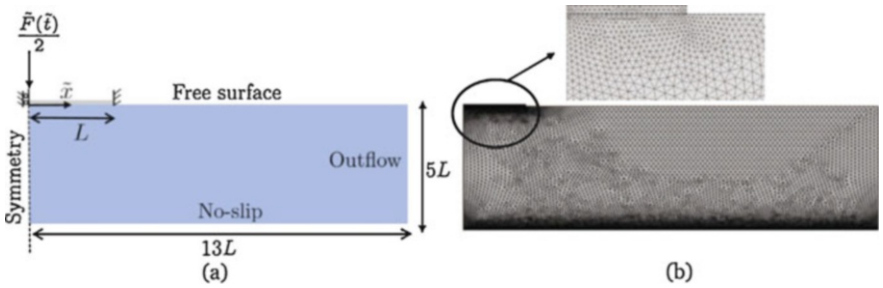


**Fig. 35** (**a**) Finite element model in COMSOL. (**b**) Computational mesh used for the structure and fluid, along with a close up of the fluid-structure interface. Reproduced from [38]

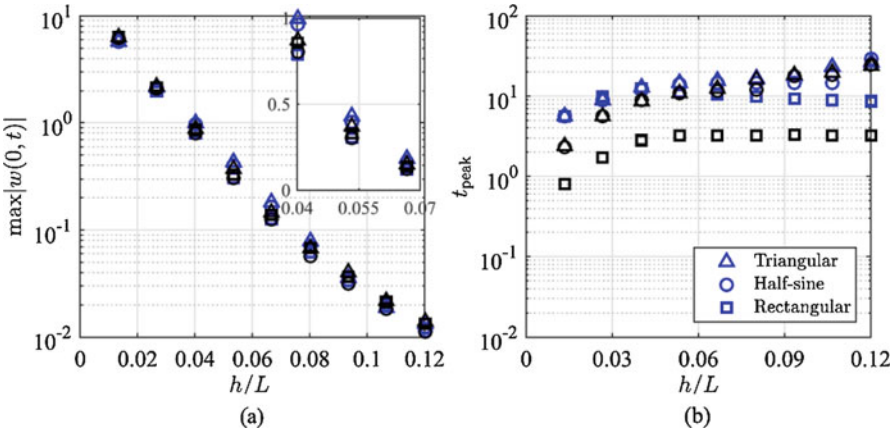


**Fig. 36** (**a**) Comparison of the maximum displacement and (**b**) peak displacement time in the presence (blue) and absence (black) of water-backing for a beam with thickness ranging from 1 to 9 mm. Reproduced from [39]

We conducted a comprehensive parametric study to ascertain the role of the thickness of the beam and explore different functional forms of the impact loading, from a square to a parabolic pulse. The key findings of the study are presented in Fig. 36, which displays the peak displacement (scaled by the thickness) and the time at which it is attained (scaled by the inverse of the fundamental radian frequency for in-air vibrations) for different thickness to length ratios.

Through the mathematical model, we confirm the intuition that water-backing has a critical role on the structural dynamics, stronger for thin beams subject to rapid pulses. Such an effect is more clear in terms of the time scale of the response (Fig. 36b), rather than the severity of the vibrations (Fig. 36a). In fact, the added mass phenomenon significantly slows down the dynamic response of the panel, especially for thin structures subject to rectangular pulses. Membrane contributes a robust stiffening effect which mitigates the severity of the response and the time at which the peak vibration is attained, as seen in the nonlinear dependence of the time scale on the thickness of the panel.

Based on this preliminary evidence, we are in the process of collecting experimental data on the impact of aluminum panels at the University of Naples. These experiments require a slight modification of the existing setup for water-backing tests, such that the panel will be clamped on two opposite sides only and the impactor will have a cylindrical shape. Notably, we are conducting these experiments utilizing different liquids, beyond water, to verify the role of the added-mass phenomenon. Collecting these data will constitute a first step toward the validation of the modeling framework for two-dimensional deformation, before expanding to three-dimensional impact and including constitutive models for the composite.

Another piece of research that is being pursued is the development of a combined particle image velocimetry/digital image correlation technique to simultaneously capture the mechanical deformation of the panel and the fluid flow. Such an analysis

is expected to aid in the extension of the model and its careful validation, by shedding light on the fluid-structure interaction from both the points of view of experimental solid and fluid mechanics.

## 5 Conclusions

Low velocity impact tests until penetration were performed on polymeric composite laminates for varying energy values. At first, we focused on the characterization of damage and on the influence of impact energy and laminate thickness on the onset and propagation of damage. Then, we examined dynamic behavior of carbon fiber reinforced plastic laminates in extreme conditions, by comparing results obtained in different temperature conditions. Results obtained from the analysis of the load displacement curve, were studied and examined within the context of existing semi-empirical models. These data are also used to support the numerical simulations presented by Porfiri in another chapter of the present book.

The internal damage was investigated through destructive and non-destructive techniques, offering insight into promising, novel experimental techniques. Results in terms of delaminated area were compared, suggesting good agreement between techniques. All the techniques evidenced the classical lobe shape of the delamination, affording simple experimental measurements. The ESPI technique, in particular, was determined to be a valid tool to investigate the impact damage on composite laminates.

Testing at low temperatures, we discovered a generally more brittle behavior with respect to experiments at room temperature. In particular, we draw the following conclusions. Higher energies were necessary to penetrate the same laminates at lower temperature, due to additional brittle damage. On the contrary, the absorbed energy was found to decrease at higher temperature, suggesting that internal damage can propagate in an easier way. Our experiments offer evidence in favor of a power law for the prediction of the penetration energy as a function of the fibre volume fraction and the impactor diameter. The brittle behaviour at low temperature was confirmed by the lower indentation depths respect to the room conditions. The indentation depth, in fact, was found to increase at higher temperature. The laminate thickness was found to be an important factor in determining changes in the damage mechanisms, by shaping the interplay between bending and shear effects. Delamination was found to be more extensive at lower temperature, although plotting the delaminated area against the maximum load, we identified a single linear trend, irrespective of the temperature.

The validation of semi-empirical models at low temperature constitutes a significant contribution of this research, toward the final aim of predicting the residual properties of a laminate after dynamic loading. Given the existing relationship between residual strength and impact energy and between indentation and nondimensional energy, it could be possible to correlate the residual strength after low velocity impacts to external damage. However, this requires knowledge o the

impactor, which might represent a limitation of the approach. Through a simple damage measurement, it could be possible to gain information about the possibility to replace a mechanical part on the structure without dismantling the whole panel.

Another central contribution of this study is the systematic analysis of the impact response of composites in the presence of water, simulating a realistic loading condition in Navy-relevant applications. Specifically, we examined three complementary scenarios. First, the case in which the panel was supported by a water layer, without clamping. Second, we clamped the panel, similar to in-air testing to perform water-backing experiments. Third, we clamped the panel at the bottom of the a tank and loaded it from its wet side. By comparing energy absorption and delamination across these different scenarios, we brought forward compelling evidence substantiating the critical role played by the fluid-structure interaction. Collectively, these experiments point at the critical role played by the added mass phenomenon in redistributing the impact throughout the panel, thereby improving energy absorption and potentially reducing the severity of the damage.

Motivated by this experimental evidence, we embarked on a modeling effort to elucidate the fluid-structure interaction that underlies water-backed impact. A preliminary mathematical model was formulated in which two-dimensional deformation of a clamped panel are examined. The model takes into account nonlinear stiffening from membrane-stretching along with non-local added mass phenomena associated with the motion of the water below the panel. The reduced-order model was validated through comparison against detailed numerical simulations on a finite element model. Future work should seek to extend the model to incorporate three-dimensional effects, as well as resolving the contact between the panel and the impactor.

**Acknowledgement** The work has been supported by the Office of Naval Research (Grant N00014-10-1-0988, N00014-18-1-2218, N00014-14-1-0380, and N62909-16-1-2220) with Dr. Y.D.S. Rajapakse as the program manager.

## References

1. Howard M, Hollaway L (1987) The characterization of the non-linear viscoelastic properties of a randomly orientated fibre/matrix composite. Composites 18:317–323
2. Shindo Y, Ueda S, Nishioka Y (1993) Mechanical behavior of woven composites at low temperatures. Fusion Eng Des 20:469–474
3. Kim MG, Kang SG, Kim CG, Kong CW (in press) Composite structures
4. Sefrani Y, Berthelot JM (2006) Temperature effect on the damping properties of unidirectional glass fibre composites. Compos Part B 37:346–355
5. Khalid A (2006) The effect of testing temperature and volume fraction on impact energy of composites. Mater Des 27:499–506
6. Ibekwe SI, Mensah PF, Li G, Pang SS, Stubblefield MA (2007) Impact and post impact response of laminated beams at low temperatures. Compos Struct 79:12–17

7. Okada T, Faudre MC, Tsuchikura N, Nishi Y (2016) Improvement of low-temperature impact value of Sandwich-structural(CFRP/ABS/CFRP) laminate plies by Homogeneous Low-EnergyElectron Beam Irradiation (HLEBI). Mater Trans 57(3):305–311
8. Kang K-w, Kim H, Chung T, Koh S (2010) Temperature effect of low velocity impact resistance of glass/epoxy laminates. Int J Mod Phys B 24(15–16):2657–2663
9. Lopresto V, Langella A, Papa I (2017) Dynamic load on composite laminates in the presence of water. Polym Eng Sci 57(6):613–620
10. Liu S, Kutlu Z, Chang FK (1993) Matrix cracking and delamination propagation in laminated composites subjected to transversely concentrated loading. J Compos Mater 27:436
11. Heimbs S, Heller S, Middendorf P, Hähnel F, Weiße J (2009) Low velocity impact on CFRP plates with compressive preload: test and modelling. Int J Impact Eng 36(10–11):1182–1193
12. Bouvet C, Rivallant S (2016) Damage tolerance of composite structures under low-velocity impact. In: Dynamic deformation, damage and fracture in composite materials and structures. Woodhead Publishing, Cambridge, pp 1–7
13. Aymerich F, Dore F, Priolo P (2008) Prediction of impact-induced delamination in cross-ply composite laminates using cohesive interface elements. Compos Sci Technol 68 (12):2383–2390
14. ABAQUS Analysis User's Manual 6.12, 2012
15. Belingardi G, Vadori R (2002) Low velocity impact tests of laminate glass–fiber–epoxy matrix composite materials plates. Int J Impact Eng 27:213–229
16. Belingardi G, Vadori R (2003) Influence of the laminate thickness in low velocity impact behaviour of composite material plate. Compos Struct 61:27–38
17. Pagliarulo V, Rocco A, Langella A, Riccio A, Ferraro P, Antonucci V, Ricciardi MR, Toscano C, Lopresto V (2015) Impact damage investigation on composite laminates: comparison among different NDT methods and numerical simulation. Meas Sci Technol 26(8):085603
18. Busse G (1979) Optoacoustic phase angle measurement for probing a metal. Appl Phys Lett 35:759–760
19. Pagliarulo V, Palummo R, Rocco A, Ferraro P, Ricciardi MR, Antonucci V (2014) Evaluation of delaminated area of polymer/carbon nanotubes fiber reinforced composites after flexural tests by ESPI, IEEE MAS Proceedings 6865922: 211–215
20. Yang SH, Sun CT (1982) In: Daniel IM (ed) Indentation law for composite materials, Composite materials: testing and design, ASTM STP 787. American society for testing and materials, Philadelphia, pp 425–449
21. Timoshenko SP (1953) Strength of materials. McGraw-Hill, New York
22. Wang H, Vu-Khanh T (1995) Fracture mechanism and mechanisms of impact-induced delamination in laminated composites. J Compos Mater 29:156–178
23. Chang FK, Choi HY, Wang HS (1990) Damage of laminated composites due to low velocity impact, 31st AIAA/ASME/ASCE/AHS/ASC structures, structures dynamics and materials conference, Long Beach, 930
24. Abrate S (2001) Modeling of impacts on composite structures. Compos Struct 51:129–138
25. Krueger (2004) Virtual crack closure technique: history, approach, and applications. Appl Mech Rev 57(2):109–143
26. Pagliarulo V, Lopresto V, Langella A, Antonucci V, Ricciardi MR, Ferraro P (2016) Non-destructive evaluation of impact damage on carbon fiber laminates: comparison between ESPI and Shearography, AIP Conference Proceedings 1740, 040002
27. Kwon YW, Owens AC (2011) Dynamic responses of composite structures with fluid–structure interaction, Advanced Composite Materials IN-TECH publisher
28. Kwon YW (2014) Dynamic responses of composite structures in contact with water while subjected to harmonic loads. Appl Compos Mater 21:227–245
29. Kwon YW, Violette MA (2012) Damage initiation and growth in laminated polymer composite plates with fluid-structure interaction under impact loading. Int J Multiphysics 6(1):29–42

30. Caprino G, Lopresto V, Scarponi C, Briotti G (1999) Influence of material thickness on the response of carbon-fabric/epoxy panels to low-velocity impact. Compos Sci Technol 59:2279–2286
31. Putić S, Stamenović M, Bajčeta B, Stajčić P, Bošnjak S (2007) The influence of high and low temperatures on the impact properties of glass–epoxy composites. J Serb Chem Soc 72(7):713–722
32. Lopresto V, Langella A (2014) Composite laminates under dynamic extreme conditions, international symposium on dynamic response and failure of composite materials, DRaF2014. Procedia Eng 88:173–179
33. Hashin Z (1980) Failure criteria for unidirectional fiber composites. J Appl Mech 47:329–334
34. Caprino G (1984) Residual strength prediction of impacted CFRP laminates. J Compos Mater 18:508–518
35. Papa I, Langella A, Lopresto V (2018) CFRP laminates impacted at low velocity: influence of the matrix and temperature, AIP Conference Proceedings, 1981
36. Jackson WC, Poe CC Jr (1993) The use of impact force as a scale parameter for the impact response of composite laminates. J Compos Tech Res 15(4):282–289
37. Lagace PA, Williamson JE, Tsang PHW, Wolf E, Thomas SA (1993) A preliminary proposition for a test method to measure (impact) damage resistance. J Reinf Plast Compos 12(5):584–601
38. Shams A, Lopresto V, Porfiri M (2017) Modeling fluid-structure interactions during impact loading of water-backed panels. Compos Struct 171:576–590
39. Wagner H (1932) Uber stoss und gleitvorgange an der oberflache von flussigkeite, ZAMM – Zeitschrift fur Ange- wandte Mathematik und. Mechanik 12(4):193–215
40. Lopresto V, Langella A, Papa I (2019) Interaction of water with carbon fiber reinforced polymer laminates under dynamic loading conditions. J Mater Eng Perform,. in press 28:3220–3227. https://doi.org/10.1007/s11665-019-03915-5
41. Lopresto V, Langella A, Papa I (2016) Residual strength evaluation after impact tests in extreme conditions on CFRP laminates. Procedia Eng 167:138–142